Engineering Fracture Mechanics 98 (2013) 109–121

Contents lists available at SciVerse ScienceDirect

Engineering Fracture Mechanics

journal homepage: www.elsevier.com/locate/engfracmech

Fracture toughness analysis of a ductile steel by means of 3D surface displacements

L.D. Paolinelli [a,*], G.E. Carr [a], N. Gubeljak [b], J. Predan [b], M.D. Chapetti [a]

[a] INTEMA, CONICET – National University of Mar del Plata, J.B. Justo 4302, (7600) Mar del Plata, Argentina
[b] University of Maribor, Faculty of Mech. Eng., Smetanova 17, SI-2000 Maribor, Slovenia

ARTICLE INFO

Article history:
Received 9 May 2012
Received in revised form 27 September 2012
Accepted 15 December 2012

Keywords:
Out-of-plane displacements
Standard fracture toughness tests
Fracture initiation
Steel
Z_a method

ABSTRACT

The standards for characterization of fracture toughness of metals are focused on the calculation of fracture parameters based only on in-plane displacements of the specimen tested. Although fracture is a three-dimensional problem, out-of-plane displacements of the specimen tested are not mentioned in those documents. Since three-dimensional displacement measurement is available, it is worth investigating its potential uses in fracture tests.

In this work, the fracture toughness of a structural steel was assessed through standard tests, measuring three-dimensional surface displacements. An alternative Crack Tip Opening Displacement calculation was introduced. The fracture initiation was inferred from the out-of-plane displacements, finding good agreement with results from R-curves.

1. Introduction

The characterization of fracture toughness of metals by means of fracture tests has been widely standardized, e.g. [1–3]. These standards are focused on the calculation of representative parameters of fracture toughness such as the Crack Tip Opening Displacement (CTOD) or the *J*-integral, based only on the in-plane displacements and the load record of the specimen tested. Subsequently, the determination of its corresponding critical toughness value is done by means of the construction and analysis of R-curves, or in some cases (e.g. brittle materials) when the maximum load is attained. Although it is well known that fracture mechanics is a three-dimensional problem, no comment or observation regarding out-of-plane displacements of the specimen tested is found in the standards.

The assessment of out-of-plane displacements in fracture mechanic tests was not frequent years ago due to the complexity involved in their in situ measurement. Optical experimental techniques such as interferometry were employed for that purpose [4,5]. The advent of digital image processing derived in the Digital Image Correlation (DIC) technique which is used jointly with a stereoscopic digital speckle photography system to measure three-dimensional surface displacement fields of loaded components [6–8]. Since this technology is widely available it is worth investigating its potential uses particularly in standard fracture toughness tests.

Most of the existing studies concerning the measurement of surface out-of-plane displacements near the crack tip in facture tests are only devoted to cases of small scale yielding in which the experimental data is correlated to analytical solutions based in the *K* dominant field and/or 3D FEM results [4,5,9–11]. Moreover, almost all of the geometries of the specimens

* Corresponding author.
E-mail address: lpaolinelli@fi.mdp.edu.ar (L.D. Paolinelli).

0013-7944/$ - see front matter © 2012 Elsevier Ltd. All rights reserved.
http://dx.doi.org/10.1016/j.engfracmech.2012.12.006

Nomenclature

a	crack length
a_b	blunting corrected crack length
a_f	final crack length
a_0	initial crack length
a_0/W	initial crack depth-to-width relation
b	remaining ligament of sample
B	sample thickness
Δa	crack length increase
δ_5	crack opening displacement defined for a gauge length of 5 mm
$\partial Z/\partial$CMOD	slope of the inward displacement Z vs. CMOD curve
E	Young's modulus
J	J-integral
K	linear elastic stress intensity factor
M	applied bending moment
M_Y	general yielding bending moment
v	Poisson's modulus
v_{pl}	plastic component of the crack mouth opening displacement
P	applied force
P_N	normalized force
r_p	plastic rotation factor
r_t	total rotation factor
S	sample span
σ_Y	yield strength
σ_T	tensile strength (engineering)
W	sample width
z	distance between load-displacement point and line of mounting of COD clip gauge
Z	out-of-plane (inwards) surface displacement
Z_a	point in Z displacement (at the pre-crack tip) vs. CMOD curve at the onset of stable crack growth

Abbreviations

ASTM	American Standards for Testing of Materials
BS	British Standard
CMOD	Crack Mouth Opening Displacement
CTOD	Crack Tip Opening Displacement
DIC	Digital Image Correlation
FEM	Finite Element Method
SENB	Single edge notched bend specimen

tested are not standard. However, metals can experience large amounts of yielding prior to initiation of stable crack growth during fracture toughness testing; thus, the available knowledge is not representative.

In this work, the fracture toughness of a structural steel with microstructural anisotropy was studied by standard tests using DIC measurements of 3D surface displacements of single edge notched bend (SENB) specimens. The critical fracture toughness was estimated by means of standard R-curves, using standard and alternative CTOD calculation and the Normalization method [12] for the crack extension determination. The out-of-plane displacements in the vicinity of the crack tip of the specimens tested were evaluated in order to infer the initiation of the stable crack growth. The outcomes were correlated with those from the R-curves and discussion was provided.

2. Materials and methods

2.1. Materials

Test samples were obtained from a railway axle of 160 mm diameter made of EA1N steel. Its chemical composition is listed in Table 1.

Tensile properties were obtained from conventional mechanical tests [13] at room temperature (24 °C) using round samples of 5 mm diameter, cut axially and transversally respect to the axle. The average measured values are listed in Table 2. No significant differences were found between samples machined in both orientations. Both specimens exhibited a Lüders plateau beyond the onset of yield stress.

Table 1
Chemical composition of the steel tested.

C	Si	Mn	P	S	Cr	Cu	Mo	Ni	V
0.4	0.5	1.2	0.02	0.02	0.3	0.3	0.08	0.3	0.06

Table 2
Tensile properties of the steel tested.

Orientation respect to axle	σ_Y (MPa)	σ_T (MPa)	E (GPa)	ν (–)	Elongation (%)
Longitudinal	307	520	210	0.3	9.4
Transverse	312	522	210	0.3	9.1

2.2. Fracture tests

Samples were cut both longitudinally, L–R, and transversally, C–L, respect to the axle axis [3] and machined into SENB specimens following standard requirements [1]. The dimensions of specimens are displayed in Fig. 1, where $W = 25$ mm, $B = 25$ mm and the span distance $S = 4W$. A crack depth-to-width relation a_0/W of 0.46–0.47 was employed in all tests.

The fracture tests were performed at room temperature (24 °C) according to [1] under displacement control (stroke velocity 1 mm/min) using an Instron® 1255 servo hydraulic testing machine with ViewMaker® 8500 + control software.

The applied force (P) and the load line displacement were discretely monitored jointly with the 3D surface displacements of the lateral surface of the specimen tested, obtaining a set of load–displacement data for each recording stage. The data sampling was performed each 2.5 s, which was low enough to prevent the loss of relevant load–displacement data during the tests performed. It is worth noting that the data sampling time of the fracture test is dependent on the loading rate, the specimen dimensions (W and B) and the material tensile properties (E and σ_Y). The Crack Mouth Opening Displacement (CMOD) required for J-integral and/or CTOD calculation was indirectly measured from 3D displacement as will be explained in detail in Section 2.4.

2.3. R-curves construction

The CTOD and the J-integral parameters were employed for critical fracture toughness determination through the construction and evaluation of R-curves. The crack extension of the tested samples was predicted for each stage of loading by means of the Normalization method using the procedure and equations given in [1] (detailed information is attached in Appendix A). The initial and final crack lengths a_0 and a_f, respectively (required as input parameters) were optically measured from the fracture surface of each tested specimen according to [1]. Where the a_0 and a_f values are calculated from the crack length measurements at nine equally spaced points along the initial (fatigue pre-crack) and the final crack fronts, respectively.

Fig. 2 shows the normalized load vs. plastic displacement of a tested sample. Fitted data and normalization function coefficients are included.

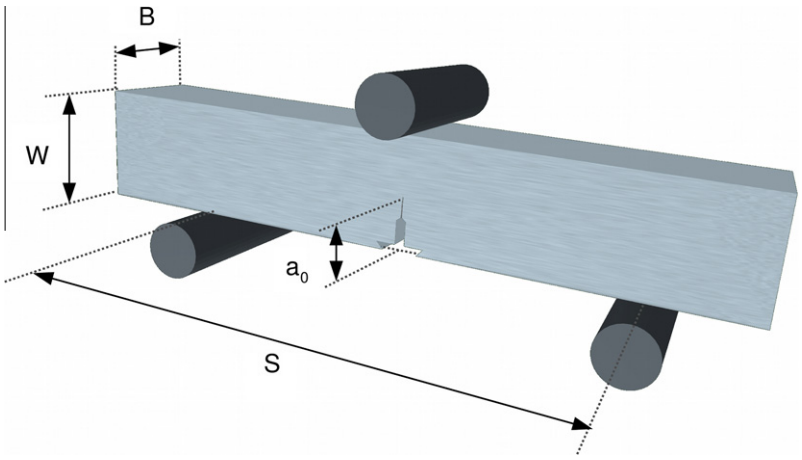

Fig. 1. Geometry and dimensions of the specimens employed.

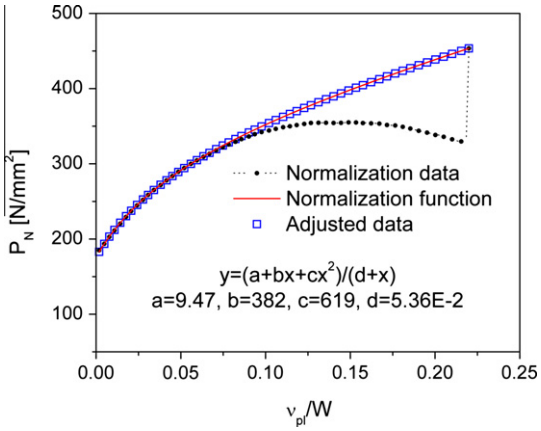

Fig. 2. Normalized load vs. plastic displacement data points from the fracture test of a longitudinal sample.

The CTOD values were computed by four different ways:

(a) Indirect measurements based on DIC results (detailed in Section 2.4).
(b) Equation given in ASTM standard E1820-11 [1] (Eq. (B.1) in Appendix B), obtained from FEM analysis, which uses *J*-integral values as input.
(c) Dawes' formula employed by the British standard BS7448-1 [2] and calculated as follows:

$$CTOD = \frac{K^2(1-\nu^2)}{2\cdot E\cdot \sigma_Y} + \frac{r_p(W-a_0)}{r_p(W-a_0)+a_0+z}\cdot \mathbf{v}_{pl} \tag{1}$$

where K is the stress intensity factor, ν is the Poisson's ratio, r_p is the plastic rotational factor (r_p = 0.4 was used [2]), v_{pl} is the plastic component of the CMOD, z is the distance of the knife edge measurement point from the notched edge on the SENB specimen.

(d) δ_5 Parameter, which was obtained from the direct measurement of the distance between two points on the lateral specimen surface, initially located at 2.5 mm from both sides of the fatigue pre-crack tip on the surface (Fig. 3) as the GKSS procedure requires [14]. However, unlike the original procedure, the measurement of the distance between the reference points (δ_5 + 5 mm) was directly performed using the DIC technique, instead of using a special clip gauge.

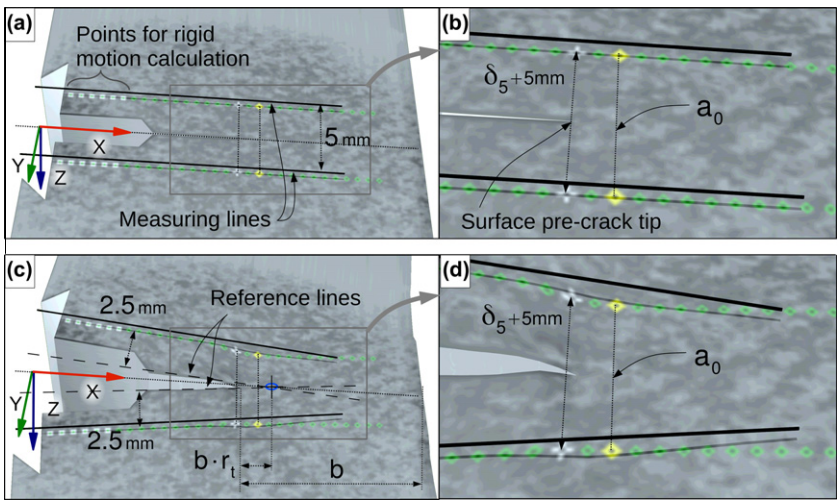

Fig. 3. Schema of the setup used for the DIC measurements on SENB specimens. (a) Specimen with speckles showing the points where 3D displacements were measured. The points were taken along two lines 2.5 mm distant from both sides of the crack. (b) Detail of the pairs of points used for the measurement of the δ_5 parameter (in white) and corresponding to the average pre-crack length position, a_0 (in yellow). (c) Deformed specimen showing the rigid rotation point. (d) Detailed view of part c, where the out-of-plane inward displacements near the crack tip can be observed. (For interpretation of the references to colour in this figure legend, the reader is referred to the web version of this article.)

2.4. Digital Image Correlation setup

Digital Image Correlation (DIC) technique was employed to calculate the spatial movement of the surface points of the specimens. For this purpose, the Aramis® GOM GmbH software and equipment were used. Post processing of the pictures generated three-dimensional data points for analysis with an acquisition precision of ±2.5 μm.

The lateral surfaces of the samples were painted with dark speckles at random against a white background. Digital photographs of the surface were taken using two cameras (left and right) prior to and throughout the bending fracture test. The DIC technique searches for the features of the painted surface in each pair of left and right camera pictures to determine the location of such points in the three-dimensional space, and hence, for matching these points between different stages throughout the test. Using this technique, any amount of points defined as zones on the surface (portions of the pictures) can be tracked throughout the fracture test.

A schema of the points of interest for measurements is shown in Fig. 3. Two groups of corresponding data points were taken along two lines (measuring lines) running parallel to the crack at distances of +2.5 mm and −2.5 mm to measure their three-dimensional position throughout the fracture test (Fig. 3a). The distance between each monitoring point along the measuring lines was 0.1 mm. The pairs of points that were located in the rigid movement portion of the samples were defined to calculate the angle of rotation of each side of the test specimen. At least six points in a span of not less than 4 mm were taken for the calculation of slopes for each line (points in white squares in Fig. 3a and c). The calculation of the slopes of the interpolating lines at each side of the crack was done using a linear least squares fit.

Subsequently, the zero crossing of two lines parallel to the interpolating lines (named as 'reference lines', dashed lines in Fig. 3c) was used to determine the total rotation factor (r_t, indicated in Fig. 3c). The variations of the distances between all the corresponding pairs of points astride the crack were calculated. Particularly, the δ_5 parameter was directly measured using the aforementioned DIC technique as shown in Fig. 3.

The CTOD (defined as method (a) in Section 2.3) was calculated as the distance along the Y axis (Fig. 3) between the corresponding points on the reference lines (dashed lines in Fig. 3c) at the initial crack length position (a_0).

Two reference points, found by extrapolation of the interpolating lines at stage zero (prior to loading) to the notched surface of the specimen, were used to calculate CMOD at each sampling stage.

Throughout the bending test, the points measured exhibited different movements regarding their position in the specimen surface. While the majority of the points of the sample surface showed in-plane movement (across XY plane), the points surrounding the crack tip showed displacements along the three axes. These out-of-plane displacements were taken as the average of the corresponding points at each side of the crack, for different positions along the X axis (crack direction) as will be shown later. The obtained out-of-plane displacements (named here 'Z displacements') were used for ductile fracture analysis.

3. Results and discussion

3.1. Fracture toughness calculation from CTOD-R curves

Fig. 4 shows CTOD-R curves for both the longitudinal and the transverse specimens, respectively. The displayed CTOD values correspond to the calculation procedure based on DIC measurements and rigid motion supposition previously introduced as definition (a) in Section 2.3. A power law fitting in the range of the experimental data values between the exclusion lines of 0.15 mm and 1.5 mm of Δa is shown on the resistance curves. The interception of the power law fitting

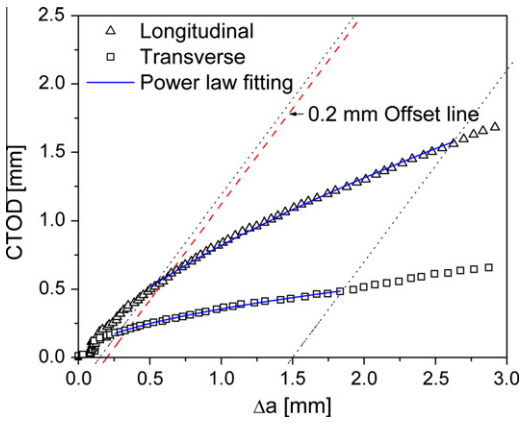

Fig. 4. CTOD-R Curves for the longitudinal and the transverse fracture samples. CTOD values obtained from indirect DIC measurements (definition a) in Section 2.3.

curve with the 0.2 mm (Δa) offset line gives the critical point in which the stable fracture growth would begin ([1], A9 and A11 sections).

Important differences are seen when comparing the CTOD values and the slopes of the CTOD-R curves for the longitudinal and the transverse specimens (Fig. 4). This behaviour would be associated to the high deformation-induced microstructural anisotropy of the tested material due to the axle manufacturing process, in which hot and cold working oriented in the longitudinal axle direction are involved. Variations in the fracture toughness values regarding the test orientation of metals with this kind of microstuctural anisotropy and discussion of its causes are reported elsewhere [15]. These issues are not addressed here since they are out of the scope of this work.

The prediction of the fracture toughness of the tested samples from CTOD-R curves was also assessed with other different standard methods for the CTOD estimation (as mentioned in Section 2.3) in order to compare and validate the CTOD calculation procedure based on DIC measurements presented in this paper (definition a) in Section 2.3.

Figs. 5 and 6 show CTOD values versus normalized CMOD values calculated by the different employed methods for the longitudinal and the transverse samples respectively. It can be noticed that CTOD values calculated from DIC indirect measurements (definition a) in Section 2.3 are somewhat in agreement with the values estimated by the other methods (E1820-11 equation, Dawes' formula and δ_5), particularly for the range of values around the fracture initiation loci predicted from CTOD-R curves. It is worth mentioning that the major discrepancies between the CTOD calculation methods are given beyond the fracture onset loci, as is the case of $CTOD_{E1820\text{-}11}$ series for the transverse samples (Fig. 6).

The average critical CTOD values for all the tested samples and the different CTOD calculation methods employed are listed in Table 3.

Fig. 7 shows the normalized applied moment (M/M_Y) versus the normalized CMOD values for the longitudinal and the transverse specimens. The general yielding moment (M_Y) for the employed specimen geometry was calculated as follows [16]:

$$M_Y = 1.456 \cdot \frac{\sigma_Y B \cdot (W - a_0)^2}{4} \tag{2}$$

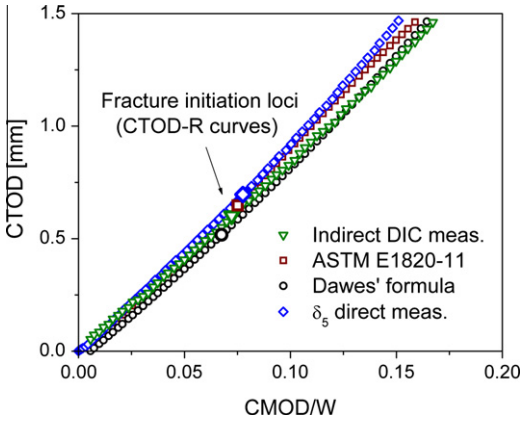

Fig. 5. CTOD calculated by different methods vs. normalized CMOD values for the longitudinal fracture samples.

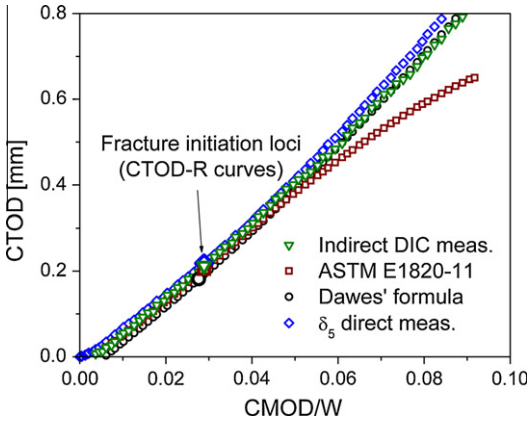

Fig. 6. CTOD calculated by different methods vs. normalized CMOD values for the transverse fracture samples.

Table 3
Critical CTOD values calculated by different methods for longitudinal and transverse samples.

Orientation respect to axle	$CTOD_{CR}$ (mm)			
	DIC indirect measurement	E1820-11 equation	Dawes' formula	δ_5 direct measurement
Longitudinal	0.55 ± 0.04	0.61 ± 0.04	0.50 ± 0.04	0.60 ± 0.08
Transverse	0.21 ± 0.01	0.21 ± 0.02	0.20 ± 0.02	0.23 ± 0.02

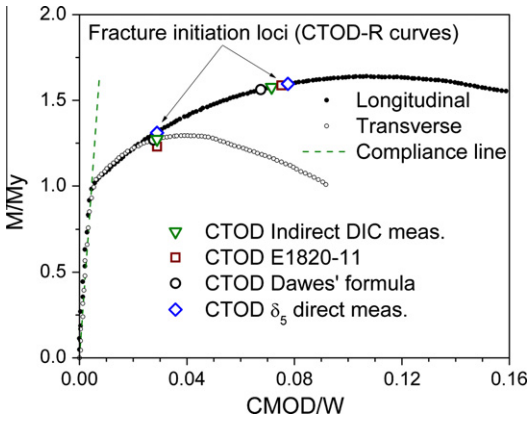

Fig. 7. Normalized applied moment vs. normalized CMOD values for the longitudinal and the transverse samples. Empty symbols indicate the predicted fracture initiation points.

The fracture initiation loci predicted from CTOD-R curves for different CTOD calculation methods are indicated with empty symbols on the load curves.

From Table 3 and Fig. 7, it can be observed that the specimens with relatively large plastic displacements before the attainment of the maximum load, as the case of the longitudinally oriented, show some discrepancies between the average critical CTOD values calculated by the different employed methods. For example, the CTOD calculated by ASTM E1820-11 is up to 20% higher than the value estimated by the Dawes' formula (BS7448-1). Recent works have shown an opposite trend for CTOD values calculated according the U.S. and the British standards for specimens of similar materials and geometry [17,18]. However, the CTOD results calculated by ASTM standards shown in both, this work and [17,18] could be non-comparable to each other. Although the same equation for CTOD calculation is used (Eq. (B.1)), there are differences in the expressions employed for the estimation of the *J*-integral. It is worth noting that the *J*-integral formula used in this work (Eq. (A.6), [1] Annex: A.1.4.2. Calculation of *J* for Bend Specimens for the Resistance Curve Test Method) is the latest reported by ASTM.

The here introduced CTOD calculation method from indirect DIC measurements predicts a critical CTOD in between the estimated by both the U.S. and the British standards, showing variations not higher than 10%. It must be noticed that the dispersion of each of these results is around 5–10%.

In the case of the transverse specimens, where the plastic displacements before the attainment of maximum load are relatively small, the CTOD calculation by indirect DIC measurements shows a very good agreement with the methods given by the standards with variations not higher than 5%, which is less than the dispersion in the results.

The measured critical CTOD-δ_5 values are relatively similar to the predicted by the other employed methods. For example, the differences of these values respect to the CTOD values calculated by indirect DIC measurements are not higher than 10% for both kinds of samples tested. Although the δ_5 method was originally proposed for thin specimens (almost straight crack front), it seems to be useful in this case of study in which relatively thick specimens are tested.

3.2. Observation of out-of-plane displacements of specimen lateral surfaces at the vicinity of the pre-crack tip

As mention in Section 1, the surface out-of-plane displacements of fracture specimens has been studied in order to infer the surface stress–strain field near the crack tip and thereby characterize the fracture behaviour of the whole specimen. In this section, the surface out-of-plane displacements of certain points at the vicinity of the pre-crack tip of standard fracture samples are empirically assessed and correlated with standard fracture parameters that describe the average through-thickness behaviour. The monitoring points under study belong to the same set of data points described in Section 2.4 (points on lines initially located at ±2.5 mm from the crack path direction).

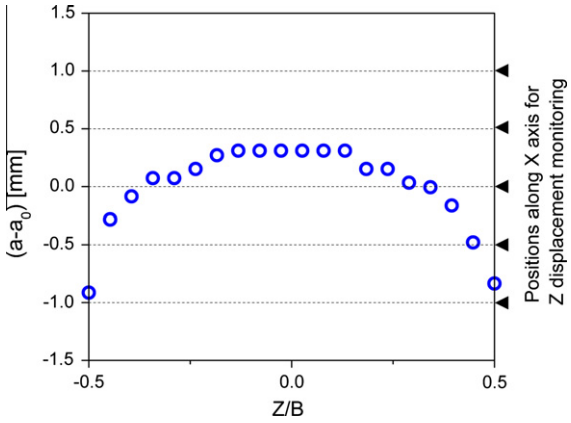

Fig. 8. Typical pre-crack front of specimens tested. Positions in *X* axis for the monitoring of *Z* displacements are indicated.

Since the prismatic specimens used in this work have curved pre-crack fronts as shown in Fig. 8, the assessment of the 3D displacements just at the surface pre-crack tip position (the only recognizable location of the pre-crack front without post-mortem analysis of the specimen) may be non-representative of the through-thickness fracture behaviour of the sample under study. For this reason, the monitoring of the out-of-plane inward displacements (*Z* displacements) was performed for a set of five different locations along the *X* direction (crack direction) comprising all the pre-crack front depth (Fig. 8): at the average pre-crack position (a_0), two at 0.5 mm and 1 mm ahead of a_0, and two at 0.5 mm and 1 mm behind a_0.

Figs. 9 and 10 show the *Z* displacements of the surface points in the neighbourhood of the pre-crack tip versus normalized CMOD values. The lateral contraction of the specimen is shown as a positive displacement value. Moreover, the normalized applied moment (M/M_Y), the crack propagation length (Δa), and the indication of the fracture initiation locus predicted by using R-curves are included in the plots for reference. The choice of the CMOD as abscissa in the *Z* displacement plots was made because the CMOD is an easy-to-measure geometric parameter that always increases during the fracture test and can be directly related to the CTOD by means of different ways as shown previously.

As the specimen is loaded, a rapid increase in side necking is observed up to the general yielding of the remaining ligament ($M/M_Y = 1$). It is worth noting that the *Z* displacements of the points located behind a_0 ($a_0 - 0.5$ mm and $a_0 - 1$ mm) are lower than those of points ahead of a_0 ($a_0 + 0.5$ mm and $a_0 + 1$ mm), which is a consequence of the constraint due to the unloaded portion of the specimen behind the pre-crack front.

Little beyond the point of general yielding is reached, the lateral contraction remains almost constant. As load increases, a partial relaxation of side necking is observed for some of the monitored points, particularly for the longitudinal samples. This effect results greater the more behind the monitored points are from a_0. However, it is not noticed for points ahead of a_0. The partial relaxation effect could be related to the yielding behaviour of the tested material, which shows a Lüders plateau in the tensile tests with an upper yielding point and subsequent yield elongation at lower stress level before the beginning of the strain hardening. This effect may lead to stress redistributions in the remaining ligament of the loaded fracture specimen and the consequent elastic partial relaxation of side necking at the vicinity of the pre-crack tip.

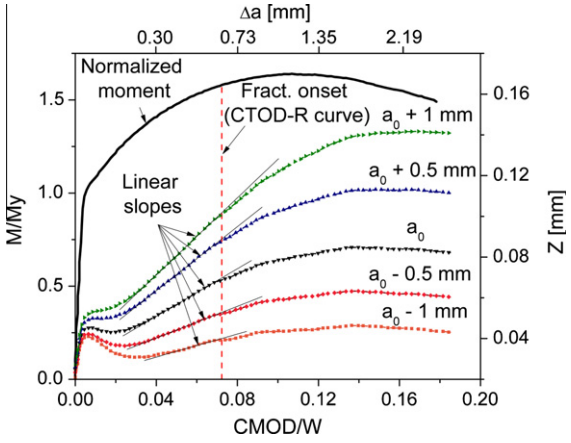

Fig. 9. Z displacements of surface points neighbouring the crack tip vs. normalized CMOD values for the longitudinal specimens.

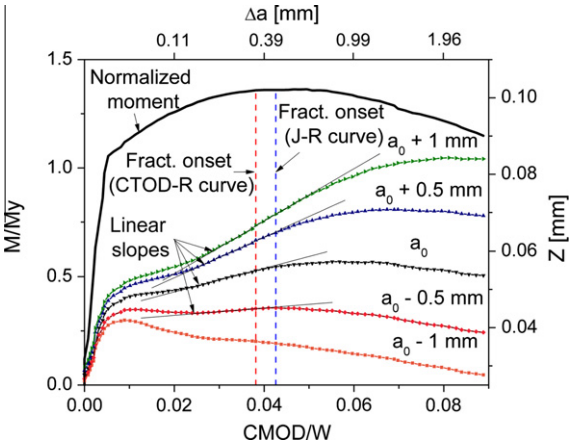

Fig. 10. *Z* displacements of surface points neighbouring the crack tip vs. normalized CMOD values for the transverse specimens.

As load (as well as the CMOD) goes on increasing beyond general yielding point, an increase of the lateral contraction is observed. This increment of the *Z* displacements respect to the CMOD (∂*Z*/∂CMOD) reaches a maximum which seems to keep constant up to a certain point. In this case of study, the sections of maximum slope ∂*Z*/∂CMOD were fitted with great accuracy using linear regression (less than 1% of error, Figs. 9 and 10). Subsequently, if the CMOD keeps increasing, the slope ∂Z/∂CMOD starts diminishing, so the *Z* displacement starts relaxing. This fact would indicate the relaxation of the stress field surrounding the monitored point, which would be caused by the fracture of the adjacent material.

While the maximum slope ∂Z/∂CMOD was found constant (linear behaviour from a certain point up to its relaxation) for these test conditions and material, more research is required to determine the rules describing this behaviour (large scale yielding). It is expected to depend not only on Young's and Poisson's moduli but also on the yield stress, hardening exponent values and specimen geometry.

From Fig. 9, it can be noticed that the relaxation points of the Z displacements corresponding to a_0 (named here for simplicity as 'Z_a') and its neighbouring positions (−1, −0.5, +0.5 and +1 mm) show good agreement with the fracture onset predicted by using the CTOD-R curve (red dashed line) for the case of the longitudinal samples tested. The CTOD calculation method employed in all the assessments done in the present section is the defined as a) in Section 2.3.

The J–R curves are also available to estimate the fracture onset in order to evaluate if the relaxation of the *Z* displacements are indicative or not of such event. However, this estimation based on *J*-integral values was not made for the case of the longitudinal samples tested, given that the majority of their *J*-integral values available for analysis were above the maximum *J*-integral capacity of the specimen that is imposed in the standard for J–R curves [1].

In the case of the transverse samples (Fig. 10), the sections of maximum growing slope ∂Z/∂CMOD of the measured *Z* displacements are shorter (in terms of CMOD values) than for the longitudinal samples, because of the earlier fracture initiation. When the *Z* displacement corresponding to a_0 is analyzed, its relaxation point does not show very good accordance with the fracture onset predicted by the CTOD-R curve (red dashed line). However, if the fracture initiation locus used as reference is estimated by using the J–R curve instead of the CTOD-R curve (both methodologies are offered in the standard E1820 [1]), the relaxation point of the *Z* displacement corresponding to a_0 agrees well with the fracture onset (blue dashed line, Fig. 10). It is worth noting that the *Z* displacements measured at the extreme points neighbouring the position of a_0 do not seem to be useful to infer the fracture initiation unlike the behaviour seen in the longitudinal samples. For example, the *Z* displacement corresponding to $a_0 - 1$ mm shows an almost continuous elastic relaxation a little beyond the general yielding point and no growing behaviour is seen. On the other hand, the *Z* displacement related to $a_0 + 1$ mm shows a growing behaviour but its relaxation point is (in terms of CMOD values) quite beyond the fracture initiation loci predicted by using both CTOD-R and J–R curves.

In view of the potential use of the *Z* displacements at the vicinity of the pre-crack tip as a tool for the estimation of ductile fracture initiation, strict analyses of their relaxation points were done for all the tested samples. For each *Z* displacement vs. normalized CMOD curve corresponding to a given specimen, the section of maximum growing slope ∂*Z*/∂CMOD was delimited and fitted with a minimum squares linear regression. When a deviation over 1% between the fit and the *Z* displacement record was found, the relaxation point (CMOD; Z pair) was established. Subsequently, the CMOD values found were directly associated to their respective CTOD values and compared with the critical CTOD values obtained from the R-curves.

Table 4 lists the average critical CTOD values determined by using the *Z* displacements at the different monitored positions neighbouring the crack tip for all the longitudinal and the transverse samples. The relative errors of these values respect to the average critical CTOD values obtained from the R-curves are also listed as reference.

The percentage error values listed in Table 4 for the case of the longitudinal samples confirm the behaviour seen in Fig. 9. The determination of the critical CTOD values by means of the relaxation point of the *Z* displacement corresponding to a_0

Table 4
Critical CTOD values determined by means of Z displacement analysis in various positions for longitudinal and transverse samples. Relative errors of this values respect to the values predicted by R-curves are added as reference.

Position in X axis	Longitudinal		Transverse			
	$CTOD_{CRref}$: 0.55 ± 0.04 mm (CTOD-R curves)		$CTOD_{CRref}$: 0.21 ± 0.02 mm (CTOD-R curves)		$CTOD_{CRref}$: 0.25 ± 0.02 mm (J–R curves)	
	$CTOD_{CR}$ (mm)	Error (%)	$CTOD_{CR}$ (mm)	Error (%)	$CTOD_{CR}$ (mm)	Error (%)
$a_0 - 1$ mm	0.57 ± 0.03	4	–	–	–	–
$a_0 - 0.5$ mm	0.57 ± 0.04	4	0.28 ± 0.02	33	0.28 ± 0.02	12
a_0	0.57 ± 0.02	4	0.26 ± 0.01	24	0.26 ± 0.01	4
$a_0 + 0.5$ mm	0.57 ± 0.04	4	0.28 ± 0.02	33	0.28 ± 0.02	12
$a_0 + 1$ mm	0.59 ± 0.03	7	0.34 ± 0.02	62	0.34 ± 0.02	35

position, above named Z_a, is very accurate if compared with the average critical CTOD estimated by using the CTOD-R curves (less than 5% error). Furthermore, it is seen that the sensitivity of the Z_a to variations in the position of the monitoring points of the Z displacements along the X axis is low enough to obtain good agreement with the reference value. Even the measurements made at $a_0 - 1$ mm (very close to the surface pre-crack tip) and at $a_0 + 1$ mm are useful for estimating the critical CTOD quite precisely.

Regarding the transverse samples, the error values in Table 4 clarify the aspects observed in Fig. 10. The Z_a analysis does not seem to estimate the critical CTOD accurately if compared with the average reference value obtained from the CTOD-R curves, since an over-prediction of at least 20% is seen. On the other hand, a good agreement is observed if the Z_a results are compared with the average critical CTOD obtained from the J–R curves (less than 5% error). The difference of almost 20% shown between the reference $CTOD_{CR}$ values obtained according the CTOD-R curve or J–R curve criteria will not be discussed here since this topic is out of the scope of this work.

It is worth noting that an important variability of the Z_a results is seen for the transverse samples if the position along X axis of the monitored points moves ahead of or behind a_0. For example, the Z_a analyses at the positions $a_0 + 0.5$ mm and $a_0 + 1$ mm (ahead of a_0) show over-predictions of 12 and 35%, respectively. The growing over-prediction error with the distance of the monitoring points ahead of a_0 (also seen for the longitudinal samples but much less pronounced) would be related to the loading effect exerted by the stressed material ahead of the pre-crack tip. This loading effect would make the relaxation point as well as the maximum of the Z displacement to move ahead (in terms of CMOD) as seen in Fig. 9 and less noticeable in Fig. 10.

An over-prediction error of 12% in the Z_a analyses of the monitoring points behind a_0 (particularly at the position: $a_0 - 0.5$ mm) is observed for the transverse samples, and could be associated with an intrinsic calculation error. In this case, the detection and accurate fit of the maximum slope $\partial Z/\partial CMOD$ (needed as reference for the determination of the relaxation point) result difficult because of its very low value and the short section (in terms of CMOD) of growing Z displacement available for analysis.

Identifying the relaxing point of the Z displacements accurately, once the fracture specimen is loaded beyond the general yielding of the remaining ligament, is easier the higher the side necking and the plastic work (and consequent size of the plastic field) that take place at the surroundings of the pre-crack tip prior to the fracture onset, as shown in the case of the longitudinal samples tested.

Although the Z_a study is based on surface displacements, the present results indicate that it can capture the average through-thickness behaviour of fracture specimens loaded in plane strain conditions. From the analysis of the measurements taken at different positions along the X axis (crack path direction), it is clear that a_0 (average X position of the pre-crack tip) is the best coordinate to characterize the fracture onset in the particular experimental setup used.

With respect to the position in the Y axis of the monitoring points of the Z displacements, the selected distance of ±2.5 mm from the surface pre-crack tip resulted to be as practical as expected, given that useful recordings of the side necking were obtained and the in-plane parameter δ_5 was also measured in the same data set. To monitor the Z displacements nearer to the crack tip in the Y axis direction could give more sensibility to the Z_a analysis, however, it could also be troublesome since the probability of finding excessively non-symmetrical displacements due to the possible deviations of the pre-crack path (up to 10° according to [2]) is higher.

3.3. General remarks

In resume, the here named 'Z_a' analysis appears to be a feasible tool for the estimation of the fracture initiation locus of ductile metals in standard fracture toughness tests, since the use of hardware and software for 3D DIC measurements is being more and more generalized in mechanical testing laboratories. Moreover, a great advantage of the Z_a analysis is that crack propagation measurements and the subsequent construction of R-curves are not needed for the assessment of the critical CTOD or J-integral values of a given material. The minimum requirements for the Z_a analysis in a fracture toughness test are:

- the capability to measure Z displacements at the vicinity of the pre-crack tip on surface,
- and the capability to measure the CMOD, which is commonly done with clip gauges or by means of in-plane DIC measurements (as was done in this work).

The knowledge of the initial crack length a_0 is also necessary for the calculation of the critical CTOD or J-integral (load–displacement record is required), thus post-mortem analysis of the fracture surface must be performed.

It is clear from the present results that a great amount of work has to be done in order to determine if the Z_a analysis can be extensively employed with satisfactory results on standard and non-standard fracture specimens. It would be interesting to characterize and analyze the out-of-plane surface displacements of specimens of different sizes (different constraint effect) as well as different geometries (as CT and MT specimens) and the existence of side grooves. Moreover, an important influence of the strain hardening exponent (Ramberg–Osgood stress–strain relation) of the tested material on the Z displacement behaviour is expected. Hence, testing of materials with different strain hardening exponents would be valuable.

3D finite element analysis involving all the issues mentioned above is also worth to be done. Particularly, the modelling of large scale yielding conditions is a concern in order to estimate plastic displacements and plastic field size, and correlate the findings with the experimental results.

4. Conclusions

In this work, CTOD-R curves for a structural steel with microstructural anisotropy were built from standard fracture toughness tests. The CTOD calculation was done using standard methods as well as a here proposed method derived from DIC measurements which involves in-plane displacements of some surface points of the specimen tested and rigid motion supposition. This alternative method proved to be very feasible, since it predicted critical CTOD values in between those estimated by both the U.S. and the British standards showing maximum variations not higher than 10%, whose were similar to the dispersion of the experimental results.

In addition, a new approach to fracture toughness testing of ductile metals was investigated. It is based on the monitoring of the surface out-of-plane displacements (here named Z displacements) at the vicinity of the pre-crack tip of the specimen tested by using the 3D DIC technique.

The initiation of stable crack growth can be directly inferred from the relaxation of the lateral contraction (shown in a Z displacement vs. CMOD plot), assessing the point in which the growing slope $\partial Z/\partial$CMOD starts diminishing. The relaxation point (CMOD; Z pair) of the Z displacement corresponding to the position of a_0 (here named: 'Z_a') can be directly associated to either a critical CTOD or J-integral value without the need for the construction of R-curves.

Although the Z_a study is based on surface displacements, it can capture the average through-thickness behaviour of fracture specimens loaded in plane strain conditions. From the experiments performed on a structural steel with microstructural anisotropy, it was found that the critical CTOD values estimated by the Z_a analysis are in good agreement with those predicted from standard R-curves. However, it was observed that the accuracy of the Z_a analysis can be strongly dependent on the position of the monitoring points, obtaining the best results for the measurements performed exactly at the position of a_0 (average X position of the pre-crack tip). It was also observed that the Z_a study is easier to perform and less position dependent (along the X axis, crack path direction) the higher the plastic work that take place at the surroundings of the pre-crack tip prior to the fracture onset of the specimen tested.

Acknowledgements

Authors wish to express their gratitude to CONICET (Argentinean Research Council) and Agencia Nacional de Promoción Científica y Tecnológica (ANPCyT), Argentina (PICT 2010 #0379) for the funding provided.

Appendix A. Normalization method

Normalization data reduction technique, as found in ASTM E1820-11 standard, applied to force vs. crack mouth opening displacement records for each specimen:

All force values P_i in the record excluding the maximum P_{max} are normalized using:

$$P_{Ni} = \frac{P_i}{WB\left(\frac{W-a_{bi}}{W}\right)^{\eta_{pl}}} \tag{A.1}$$

where a_{bi} is the blunting corrected crack size at the ith data point, calculated by:

$$a_{bi} = a_0 + \frac{J_i}{2\sigma_Y} \tag{A.2}$$

with J_i calculated using:

$$J_i = \frac{K_i^2(1-\nu^2)}{E} + J_{pli} \tag{A.3}$$

The values K_i and J_{pli} are calculated using the following equations with the initial crack size a_0:

$$K_i = \left[\frac{P_i \cdot S}{(B \cdot B_N)^{1/2} W^{3/2}}\right] \cdot f(a_i/W) \tag{A.4}$$

where S is the span length equivalent to $4W$, B_N is the net specimen thickness that is equal to B if no side grooves are present.

$$f(a_i/W) = \frac{3\left(\frac{a_i}{W}\right)^{1/2} \cdot \left[1.99 - \left(\frac{a_i}{W}\right)\left(1 - \frac{a_i}{W}\right)\left(2.15 - 3.93\left(\frac{a_i}{W}\right) + 2.7\left(\frac{a_i}{W}\right)^2\right)\right]}{2\left(1 + 2\frac{a_i}{W}\right)\left(1 - \frac{a_i}{W}\right)^{3/2}} \tag{A.5}$$

$$J_{pl(i)} = \left[J_{pl(i)} + \left(\frac{\eta_{pl(i-1)}}{b_{(i-1)}}\right)\left(\frac{A_{pl(i)} - A_{pl(i-1)}}{B_N}\right)\right] \cdot \left[1 - \gamma_{pl(i-1)}\left(\frac{a_{(i)} - a_{(i-1)}}{b_{(i-1)}}\right)\right] \tag{A.6}$$

where

$$b_i = W - a_i$$

$$\eta_{pl(i-1)} = 3.667 - 2.199\left(\frac{a_{(i-1)}}{W}\right) + 0.437\left(\frac{a_{(i-1)}}{W}\right)^2; \tag{A.7}$$

$$\gamma_{pl(i-1)} = 0.131 - 2.131\left(\frac{a_{(i-1)}}{W}\right) - 1.465\left(\frac{a_{(i-1)}}{W}\right)^2 \tag{A.8}$$

The quantity $A_{pl(i)} - A_{pl(i\text{-}1)}$ is the increment of plastic area under the chosen force vs. plastic displacement record between lines of constant plastic displacement at points i – 1 and i. The quantity $J_{pl(i)}$ represents the total crack-growth corrected plastic J at point i and is obtained in two steps by first incrementing the existing $J_{pl(i\text{-}1)}$ and then by modifying the total accumulated result to account for the crack growth increment.

The quantity $A_{pl(i)}$ can be calculated from the following equation:

$$A_{pl(i)} = A_{pl(i-1)} + \lfloor P_{(i)} + P_{(i-1)} \rfloor \lfloor v_{pl(i)} - v_{pl(i-1)} \rfloor / 2 \tag{A.9}$$

where $v_{pl(i)} = v_{(i)} - (P_{(i)} \cdot C_{(i)})$ is the plastic part of the crack mouth opening displacement, with $C_{(i)} = (\Delta v/\Delta P)_{(i)}$, corresponding to the current crack size, $a_{(i)}$.

These values can be obtained with:

$$C_{(i)} = \frac{6S}{EWB_e}\left(\frac{a_i}{W}\right) \cdot \left[0.76 - 2.28\left(\frac{a_i}{W}\right) + 3.87\left(\frac{a_i}{W}\right)^2 - 2.04\left(\frac{a_i}{W}\right)^3 + \frac{0.66}{(1 - a_i/W)^2}\right] \tag{A.10}$$

where

$$B_e = B - (B - B_N)^2/B$$

Each crack mouth displacement is normalized for finding a normalized plastic displacement:

$$v'_{pli} = \frac{v_{pli}}{W} = \frac{v_i - P_i C_i}{W} \tag{A.11}$$

where C_i is the specimen elastic load-line compliance based of the crack size a_{bi} which can be calculated using the preceding equations.

The final measured crack size a_f must be used for normalizing the final force displacement pair of data using the same equations as above. A line should be drawn from the final normalized force vs. displacement data pair and tangent to the normalized force vs. crack mouth opening displacement curve. All data between the last data pair and the tangency point must be not taken into account for the normalization function fit. So should be done to data with $v_{pli}/W \leqslant 0.001$. The following function can be used to fit the remaining data:

$$P_N = \frac{a + b \cdot v'_{pl} + c \cdot v'^2_{pl}}{d + v'_{pl}} \tag{A.12}$$

where a, b, c and d are fitting coefficients.

The method requires all data (P_{Ni}, v_{pli}/W, a_i) to lie on the previous equation, therefore, an iterative algorithm is used. It starts with finding the normalized force and displacement for $a = a_0$ for the first data point with $v_{pli}/W \geqslant 0.002$. Adjustment must be made to the crack size until the measured P_{Ni} and the functional value of P_N are within ±0.1%. For each subsequent data pairs same process is needed.

Appendix B. CTOD calculation by means of *J*-integral values

$$CTOD_{\mathbf{i}} = \frac{J(a_{\mathbf{i}})}{m_{\mathbf{i}} \cdot \sigma_{\mathbf{y}}} \tag{B.1}$$

where

$$m_{\mathbf{i}} = A_0 - A_1 \cdot \left(\frac{\sigma_Y}{\sigma_T}\right) + A_2 \cdot \left(\frac{\sigma_Y}{\sigma_T}\right)^2 - A_3 \cdot \left(\frac{\sigma_Y}{\sigma_T}\right)^3 \tag{B.2}$$

$$A_0 = 3.18 - 0.22 \cdot \left(\frac{a_i}{W}\right)$$

$$A_1 = 4.32 - 2.23 \cdot \left(\frac{a_i}{W}\right)$$

$$A_2 = 4.44 - 2.29 \cdot \left(\frac{a_i}{W}\right)$$

$$A_3 = 2.05 - 1.06 \cdot \left(\frac{a_i}{W}\right)$$

This calculation of $CTOD_i$ requires $\sigma_T/\sigma_Y \geqslant 0.5$.

References

[1] ASTM E1820-11, Standard test method for measurement of fracture toughness. West Conshohocken, PA, USA. ASTM International; 2011.
[2] BS 7448-1. Fracture mechanics toughness tests – Part 1: method for determination of Klc, critical CTOD and critical J values of metallic materials. London, UK. British Standard Institute; 2002.
[3] ASTM E399-90, Standard test method for plane strain fracture toughness of metallic materials. West Conshohocken, PA, USA. ASTM International; 1997.
[4] Humbert L, Valle V, Cottron M. Experimental determination and empirical representation of out-of-plane displacements in a cracked elastic plate loaded in mode I. Int J Solids Struct 2000;37:5493–504.
[5] Pfaff RD, Washabaugh PD, Knauss WG. An interpretation of Twyman-Green interferograms from static and dynamic fracture experiments. Int J Solids Struct 1995;32:939–55.
[6] Orteu J-J. 3-D computer vision in experimental mechanics. Optics Lasers Engng 2009;47:282–91.
[7] M.A. Sutton, J.-J. Orteu, H.W. Schreier, M.A. Sutton, J.-J. Orteu, H.W. Schreier. 1st. Amsterdam: Springer; 2009.
[8] Synnergren P, Sjödahl M. A stereoscopic digital speckle photography system for 3-D displacement field measurements. Optics Lasers Engng 1999;31:425–43.
[9] Barranger Y, Doumalin P, Dupre J-C, Germaneau A, Hedan S, Valle V. Evaluation of three-dimensional and two-dimensional full displacement fields of a single edge notch fracture mechanics specimen, in light of experimental data using X-ray tomography. Engng Fract Mech 2009;76:2371–83.
[10] Codrington J, Kotousov A, Ho SY. Out-of-plane stress and displacement for through-the-thickness cracks in plates of finite thickness. J Mech Mater Struct 2008;3:261–70.
[11] Yoneyama S, Ogawa T, Kobayashi Y. Evaluating mixed-mode stress intensity factors from full-field displacement fields obtained by optical methods. Engng Fract Mech 2007;74:1399–412.
[12] Landes JD, Zhou Z, Lee K, Herrera R. Normalization method for developing J–R curves with the LMN function. J Test Eval 1991;19:305–11.
[13] ASTM E8/E8M-11. Standard test methods for tension testing of metallic materials. West Conshohocken, PA, USA. ASTM International; 2011.
[14] K.-H. Schwalbe, J. Heerens, U. Zerbst, H. Pisarski, M. Koçak. EFAM-GTP 02, The GKSS test procedure for determining the fracture behaviour of materials. 2nd issue. GKSS, Report 2002/24; 2002.
[15] R.W. Hertzberg, R.W. Hertzberg. 3rd. New York: John Wiley & Sons; 1989.
[16] Kolednik O. On the calculation of COD from the clip-gauge displacement in CT and bend specimens. Engng Fract Mech 1988;29:173–88.
[17] Kayamori Y, Inoue T, Tagawa T. Transformation of BS7448-CTOD to ASTM E1290-CTOD. J Press Vessel Technol 2010;132:041401–7.
[18] Tagawa T, Kayamori Y, Ohata M, Handa T, Kawabata T, Yamashita Y, et al. Comparison of CTOD standards: BS 7448-Part 1 and revised ASTM E1290. Engng Fract Mech 2010;77:327–36.